# Advance Access publication 2021 August 13

# Large-scale magnetic field saturation and the Elsasser number in rotating spherical dynamo models

Ryan J. Orvedahl , 1 Nicholas A. Featherstone and Michael A. Calkins 3

- <sup>1</sup>Department of Astrophysical & Planetary Sciences, University of Colorado Boulder, Boulder, CO 80309-0391, USA
- <sup>2</sup>Southwest Research Institute, Boulder, CO 80302, USA

Accepted 2021 August 6. Received 2021 August 2; in original form 2021 July 2

#### **ABSTRACT**

Numerical simulations are used to investigate large-scale (mean) magnetic field generation in rotating spherical dynamos. Beyond a certain threshold, we find that the magnitude of the mean magnetic field becomes nearly independent of the system rotation rate and buoyancy forcing. The analysis suggests that this saturation arises from the Malkus-Proctor mechanism in which a Coriolis-Lorentz force balance is achieved in the zonal component of the mean momentum equation. When based on the large-scale magnetic field, the Elsasser number is near unity in the saturated regime. The results show that the large and small magnetic field saturate via distinct mechanisms in rapidly rotating dynamos, and that only the axisymmetric component of the magnetic field appears to follow an Elsasser number scaling.

**Key words:** convection – dynamo – magnetic fields – MHD – methods: numerical.

# 1 INTRODUCTION

The Sun and the majority of Solar System planets possess global, or large-scale, magnetic fields that are sustained by a convectiondriven dynamo operating within their interiors (e.g. Jones 2011). Observations show variability in both the magnitude and structure of these fields. Whereas Mercury, Earth, and the gas giant planets Jupiter and Saturn have predominantly dipolar magnetic fields that show preferential alignment with the planetary rotation axis, Uranus and Neptune have more complex, multipolar fields (Stanley & Glatzmaier 2010). Understanding the underlying physical processes and parameters that control both the structure and amplitude of these self-generated magnetic fields are two fundamental goals of dynamo theory. The present work uses numerical simulations to explore the behaviour of the large-scale magnetic field for varying rotation rates and buoyancy forcing.

The magnitude of a dynamo generated magnetic field is thought to be related either to the dominant forces in the fluid region, or to the power that is available to convert kinetic energy into magnetic energy (Christensen 2010). We refer to these two possibilities as the force balance hypothesis, and the energy hypothesis, though they need not be mutually exclusive (e.g. Christensen & Aubert 2006). The Coriolis force is known to play an important role in the generation of large-scale magnetic fields, and the force balance hypothesis assumes that the magnetic field strength is such that the Lorentz force is comparable in magnitude to the Coriolis force (Stevenson 1979). In contrast, the energy hypothesis assumes that the magnetic field strength is controlled by the power provided by the buoyancy force (Christensen & Aubert 2006). Since the Coriolis force does no work, it does not directly enter into the energy hypothesis.

Dynamos are commonly distinguished by comparing the typical length scales that characterize the magnetic and velocity fields (Tobias 2021). Large-scale dynamos have magnetic field length scales that are large relative to the typical scales of the velocity field. In contrast, small-scale dynamos are dominated by magnetic field scales that are comparable to, and smaller than the velocity length scales (e.g. Yan, Tobias & Calkins 2021). While dynamos are often characterized by a range of length scales, it is generally assumed that a dynamo is large-scale if the magnetic field is energetically dominated by the dipolar component in spherical geometries.

The force balance in rotating dynamos can depend on the length scale under consideration. Simulations show that the large-scale force balance in rotating convection-driven dynamos is thermal wind, i.e. the mean (azimuthally averaged) Coriolis force is comparable to both the mean pressure gradient force and the mean buoyancy force (Aubert 2005; Wicht & Christensen 2010; Sheyko et al. 2018). In contrast, the force balance on the small, fluctuating convective length scale is geostrophic: the fluctuating Coriolis force is balanced by the fluctuating pressure gradient force. The fluctuating Lorentz force enters a second, subdominant balance along with the ageostrophic fluctuating Coriolis force and the fluctuating buoyancy force (Yadav, Gastine & Christensen 2016; Aubert, Gastine & Fournier 2017; Schaeffer et al. 2017). These observations suggest that the mechanism(s) responsible for the strength of the magnetic field might also be scale dependent. Indeed, Malkus & Proctor (1975) showed that a large-scale magnetic field can saturate through the formation of a corresponding large-scale flow.

Dynamo models find that for a fixed rotation rate, the magnetic field shows a relatively sudden transition from a dipole dominated state to a multipolar state as the buoyancy force is increased. Moreover, Kutzner & Christensen (2002) found that, for certain parameter values, the energy contained within the dipole component of the magnetic field reaches a regime in which it no longer increases

<sup>&</sup>lt;sup>3</sup>Department of Physics, University of Colorado Boulder, Boulder, CO 80309-0390, USA

<sup>\*</sup> E-mail: ryan.orvedahl@colorado.edu

with the buoyancy force, but instead shows a slight decrease at the investigated rotation rate, followed by a sudden drop in magnitude that is associated with the change from a dipolar dominant state to a multipolar state.

In the present work, we investigate the behaviour of the axisymmetric (mean) component of the magnetic field in spherical dynamo models. Our findings show that the mean magnetic field reaches a regime in which it no longer increases with increasing buoyancy forcing, and is approximately independent of the system rotation rate. The analysis suggests that this phenomenon is related to the force balance in the mean zonal momentum equation. In this sense, the force balance hypothesis is observed to hold for the large-scale magnetic field since it is observed to become nearly independent of the buoyancy forcing beyond a certain threshold. This saturation of the mean magnetic field is consistent with the Malkus-Proctor mechanism.

We discuss the model setup and mean field decomposition in Section 2. Results are discussed in Section 3, followed by a discussion in Section 4.

#### 2 METHODS

We investigate convection-driven dynamos in a spherical shell with inner radius  $r_i$  and outer radius  $r_o$ , that rotates with angular frequency  $\Omega$ . The fluid is Oberbeck-Boussinesq with density  $\rho$ , thermal expansion coefficient  $\alpha$ , thermal diffusivity  $\kappa$ , kinematic viscosity  $\nu$ , and magnetic diffusivity  $\eta$ . The shell thickness is given by  $D = r_o - r_i$ , the gravitational acceleration at the outer boundary is denoted  $g_o$ , and the temperature difference between the inner and outer boundaries is  $\Delta T$ . The non-dimensional control parameters are the Rayleigh number (Ra), the Ekman number (Ek), the thermal Prandtl number (Pr), the magnetic Prandtl number (Pm), and the aspect ratio ( $\chi$ ), defined by, respectively,

$$Ra = \frac{\alpha g_0 \Delta T D^3}{\nu \kappa}, \quad Ek = \frac{\nu}{\Omega D^2}, \quad Pr = \frac{\nu}{\kappa}, \quad Pm = \frac{\nu}{\eta}, \quad \chi = \frac{r_i}{r_o}.$$

The non-dimensionalization is carried out using the shell depth D, large-scale viscous diffusion time  $D^2/\nu$ , pressure scale  $\mathcal{P}=\rho\nu\Omega$ , and magnetic field scale  $\mathcal{B}^2=\mu_0\rho\eta\Omega$ , where  $\mu_0$  is the vacuum permeability.

To compare cases with different Ekman numbers we use the asymptotically rescaled, or reduced, Rayleigh number (e.g. Julien, Knobloch & Werne 1998; Jones, Soward & Mussa 2000) defined as

$$\widetilde{Ra} = RaEk^{4/3}.$$
 (2)

In the limit  $Ek \rightarrow 0$ , we expect the dynamics to depend on Ra, rather than Ra and Ek independently.

We use no-slip, isothermal, and electrically insulating boundary conditions. The governing equations are solved numerically using the pseudospectral code Rayleigh (Featherstone & Hindman 2016; Matsui et al. 2016). In all simulations presented here, we fix  $\chi=0.35$  and Pr = 1, while varying Ra, Ek, and Pm. All statistics are computed from statistically stationary states. The most extreme simulation with Ek =  $3 \times 10^{-6}$  and Ra  $\approx 40$  use a resolution of N=180 Chebyshev polynomials in radius and a maximum spherical harmonic degree  $\ell_{\rm max}=383$ . A subset of these simulations was utilized in another recent study (Calkins, Orvedahl & Featherstone 2021).

We decompose all variables into axisymmetric (mean) and nonaxisymmetric (fluctuating) components. For instance, the magnetic field is decomposed according to

$$\mathbf{B}(\mathbf{r},t) = \overline{\mathbf{B}}(\mathbf{r},\theta,t) + \mathbf{B}'(\mathbf{r},t), \tag{3}$$

where the overline denotes an average in longitude ( $\phi$ ). The mean and fluctuating magnetic energies are then defined as, respectively,

$$\overline{E}_{\text{mag}} = \left[ \frac{1}{2\text{PmEk}} \left| \overline{\boldsymbol{B}}(\boldsymbol{r}, t) \right|^{2} \right], \quad E'_{\text{mag}} = \left[ \frac{1}{2\text{PmEk}} \left| \boldsymbol{B}'(\boldsymbol{r}, t) \right|^{2} \right],$$
(4)

where the square brackets indicate a time and volume average over the entire domain.

The mean and fluctuating magnetic field power spectra are computed according to

$$\overline{\mathcal{P}}_{B} = \left\{ \left| \overline{\boldsymbol{B}}_{\ell}^{m=0}(r,t) \right|^{2} \right\}, \qquad \mathcal{P}_{B}' = \left\{ \sum_{m \neq 0} \left| \boldsymbol{B}_{\ell}'^{m}(r,t) \right|^{2} \right\}, \qquad (5)$$

where  $B_\ell^m$  denotes a (complex) spherical harmonic coefficient of degree  $\ell$  and order m. The curly braces indicate an average over time and radius. The spectra showed only small variations with depth, therefore the radial average involved 14 radial grid points, evenly spaced across the shell depth.

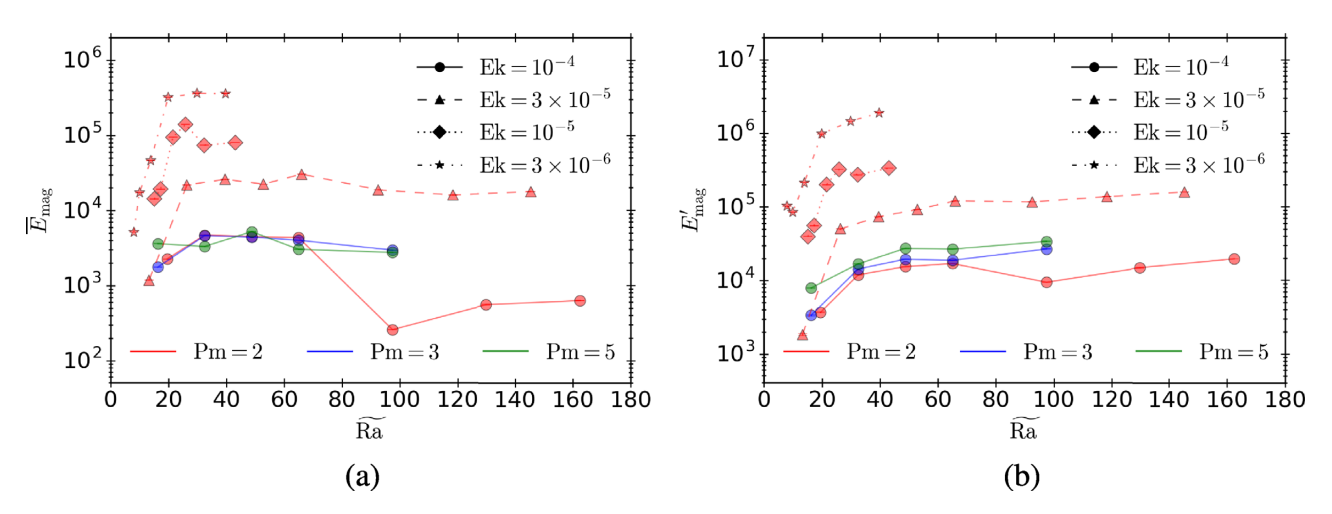
#### 3 RESULTS

Fig. 1 shows the magnetic energy decomposed into (a) mean and (b) fluctuating components. At all values of Ek, the total magnetic energy (not shown) grows as the Rayleigh number is increased, primarily owing to contributions from  $E'_{mag}$ . For smaller values of  $\widetilde{Ra}$ , we find that  $\overline{E}_{mag}$  increases with  $\widetilde{Ra}$  until transitioning to a regime in which it remains approximately constant. We refer to the latter state as the saturated mean field regime. The transition to the saturated regime occurs around Ra  $\approx 20-35$  for all Ekman numbers investigated here, though the data shows a trend that smaller Ekman numbers saturate for smaller values of Ra. In addition to these first two regimes, the largest Ekman number case of Ek =  $10^{-4}$  and Pm = 2 shows an abrupt transition to a state that is characterized by a small mean magnetic energy; this regime represents the transition to a multipolar dynamo discussed previously (Kutzner & Christensen 2002; Christensen & Aubert 2006; Soderlund, King & Aurnou 2012).

Although both the mean and fluctuating magnetic energies increase with decreasing Ekman number, this increase is due to the prefactor, 1/(PmEk), in the definition of the magnetic energy. A commonly employed non-dimensional parameter for characterizing the strength of dynamo generated magnetic fields is the Elsasser number,

$$\Lambda = \frac{B^2}{2\mu_0 \rho \eta \Omega},\tag{6}$$

though other definitions are also used (e.g. Soderlund et al. 2012, 2015; Aurnou & King 2017). In our non-dimensional units, the (squared) magnetic field strength can be recast in Elsasser number units by dividing by a factor of two and an overline is used to emphasize it is based on the mean magnetic field only. Thus, we compute the mean Elsasser number as  $\overline{\Lambda} = [\overline{B}^2/2]$ . As Fig. 2(a) demonstrates, the mean Elsasser number is approximately unity and shows a very weak dependence on the Ekman number, where it is plotted as a function of the global Rossby number, Ro  $\equiv \mathcal{U}/(\Omega D)$ , where  $\mathcal{U}$  is a characteristic flow speed computed as a root mean square (rms) of the full velocity over the entire domain. Open symbols



**Figure 1.** Magnetic energy for all simulations as a function of reduced Rayleigh number, Ra: (a) mean magnetic energy; and (b) fluctuating magnetic energy. The symbols and line styles correspond to the Ekman numbers, and the colors indicate the magnetic Prandtl number. Mean magnetic energy increases with Ra until saturating at an Ek-dependent value of Ra. Fluctuating magnetic energy shows no such behaviour and continues to increase with Ra.

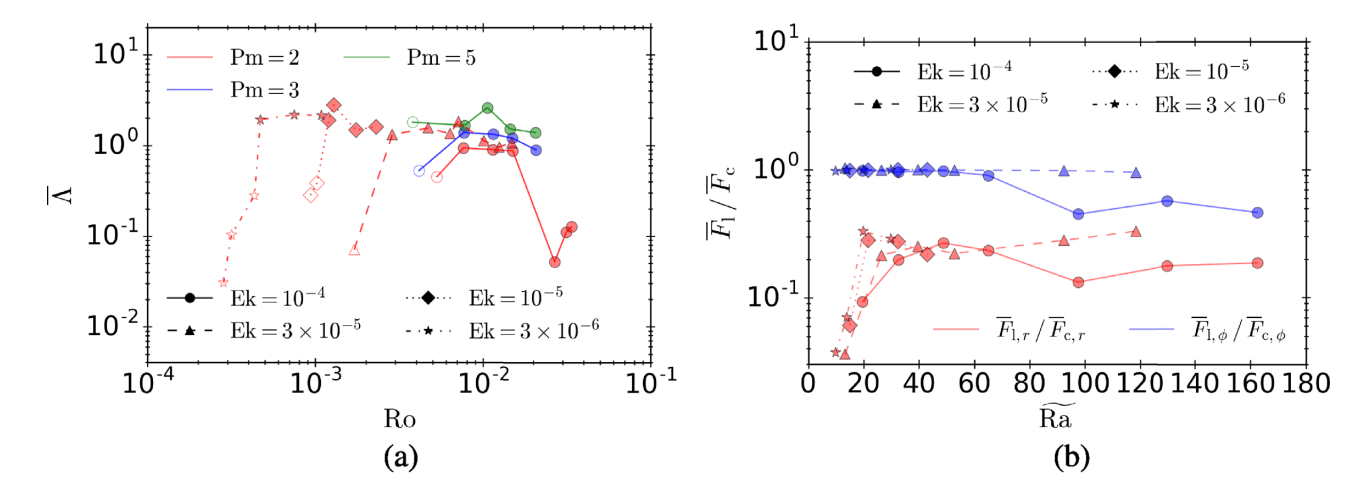


**Figure 2.** (a) The mean Elsasser number for all cases as a function of the Rossby number. Solid (open) symbols indicate cases that are in the saturated (unsaturated) regime. The mean Elsasser number saturates at a value of roughly unity for all models in the saturated regime, with the exception of the three high-Ro, multipolar cases that use  $Ek = 10^{-4}$ . (b) Ratios of the mean Lorentz force to the mean Coriolis force for both the radial and zonal components. Mean Coriolis and mean Lorentz forces are of roughly the same amplitude in the zonal direction for all models, with the exception of the three high-Ro, multipolar cases. In the radial direction, the mean Lorentz force is typically an order of magnitude smaller than the mean Coriolis force.

are used to denote field strengths prior to the saturated regime; we find that the onset of the saturated regime occurs at smaller Rossby number as Ek is reduced, implying that this regime occurs over an increasingly larger range of  $\widehat{Ra}$ . This finding suggests that natural systems are likely in the saturated mean field regime since they are characterized by (Ek, Ro)  $\ll 1$  and  $\widehat{Ra} \gg 1$ . We observe a slight increase in  $\overline{\Lambda}$  with increasing Pm and decreasing Ek; these results suggest that the natural dynamo regime (Ek, Pm)  $\ll 1$  will maintain order unity mean Elsasser numbers.

Provided that the Rossby number is not too large, the leading order mean force balance in the zonal direction is between the Coriolis force and the Lorentz force (Aubert 2005; Wicht & Christensen 2010; Sheyko et al. 2018). However, the zonal component of the Lorentz force is measurably smaller than the leading order forces in the meridional components of the mean momentum equation so that a fully magnetostrophic large-scale force balance is not present (Calkins et al. 2021). Instead, we refer to this balance as semi-magnetostrophic. To illustrate these balances, we compute the ratio

of the Lorentz and Coriolis forces component-wise according to

$$\frac{\overline{F}_{l,r}}{\overline{F}_{c,r}} = \frac{\left\langle \left( \overline{J} \times \overline{B} \right)_r \right\rangle}{\left\langle 2 \operatorname{Pm} \left( \overline{u} \times \widehat{z} \right)_r \right\rangle}, \qquad \frac{\overline{F}_{l,\phi}}{\overline{F}_{c,\phi}} = \frac{\left\langle \left( \overline{J} \times \overline{B} \right)_{\phi} \right\rangle}{\left\langle 2 \operatorname{Pm} \left( \overline{u} \times \widehat{z} \right)_{\phi} \right\rangle}, \tag{7}$$

where the angled brackets indicate an rms over the whole domain. Fig. 2(b) shows both of these force ratios. When based on the radial components, the force ratio is less than unity, showing that the Lorentz force is always smaller than the Coriolis force in the radial component of the mean momentum equation. In the zonal direction, the force ratio is approximately unity for the rapidly rotating cases, indicating that the force balance hypothesis is valid within the saturated mean field regime provided Ro is sufficiently small.

The mean Lorentz force consists of two components: the 'mean-mean' contribution  $\overline{J} \times \overline{B}$  and the 'eddy-eddy' term  $\overline{J'} \times \overline{B'}$ . Fig. 3 shows meridional views of the time averaged zonal components of

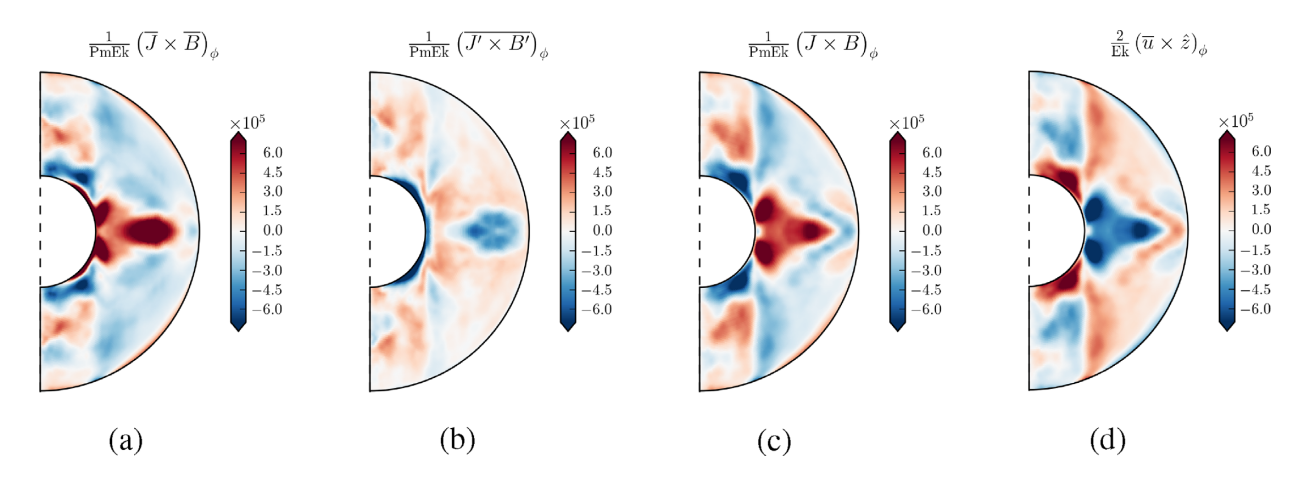


Figure 3. Balance between mean Lorentz and Coriolis force in the zonal direction for  $Ek = 10^{-5}$ , Ra = 21.5, and Pm = 2. (a) The mean–mean contribution to the mean Lorentz force, (b) the eddy-eddy term, (c) the total mean Lorentz force, and (d) the Coriolis force. The Coriolis force is largely balanced by the Lorentz force, due mainly to contributions from the mean magnetic field, though fluctuating magnetic fields do still contribute.

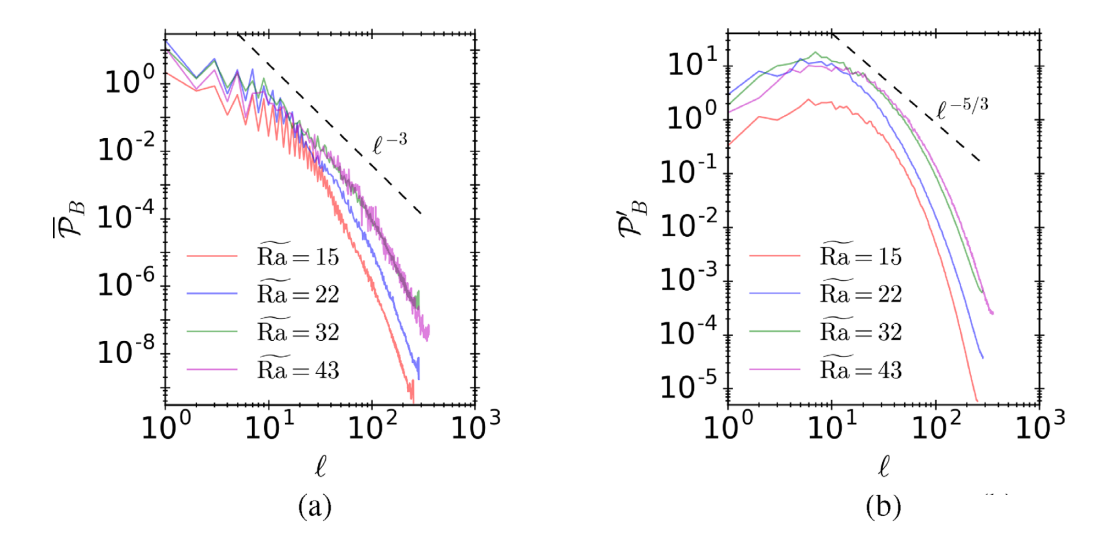


Figure 4. Power spectra for the (a) mean and (b) fluctuating component of the magnetic field. Only a subset of cases with  $Ek = 10^{-5}$  and Pm = 2 are shown. For the mean magnetic field, the power grows with increasing Ra until a critical value of Ra = 32, beyond which, the spectral shape and amplitude remain relatively unchanged. This behaviour is not observed in the spectra associated with the fluctuating magnetic field.

the mean Lorentz force as well as the zonal Coriolis force for the case with  $Ek = 10^{-5}$  and Ra = 21.5. To accelerate convergence of the time averages, we treated data in the northern and southern hemispheres as unique statistical realizations, reflected the data about the equatorial plane, and computed the resulting average. The trend toward an equatorially symmetric state was verified by averaging over increasing time intervals. In general, the relationship between these two components of the mean Lorentz force is complicated; there are regions in which they are of the same sign and regions where they are of opposite sign. However, both terms are of comparable size and are both necessary to balance the mean Coriolis force.

Fig. 4 shows the power spectra for the (a) mean and (b) fluctuating components of the magnetic field. The mean magnetic field spectra are dominated by the dipolar component that is roughly an order of magnitude larger than the  $\ell=3$  octopole component. The mean magnetic field shows larger contributions from odd spherical harmonics, consistent with a largely equatorially antisymmetric configuration. Within the saturated field regime, the dipole component saturates with increasing Ra. The spectra for Ra = 32 and Ra = 43 are nearly

the same, even for large values of  $\ell$ . This result suggests that the near saturation of the dipole contribution observed by Kutzner & Christensen (2002) is robust across all  $\ell$ , implying that the total mean field saturates, not just a particular value of  $\ell$ . In contrast to the mean field, as Ra increases, the power in the fluctuating magnetic field (Fig. 4b) increases at all spatial scales for smaller values of Ra. Beyond Ra  $\approx$  22, the low- $\ell$  power begins to decrease, whereas the high- $\ell$  power continues to increase slightly.

### 4 DISCUSSION AND CONCLUSIONS

Self-generated magnetic fields are common throughout the Solar System and beyond. Understanding the processes that control the strength of these fields and their structure are two basic problems in dynamo theory. Although numerical simulations cannot currently be used to study dynamos with parameter values comparable to those in natural systems, parameter surveys with these models can be used to identify asymptotic behaviour that allow for extrapolation to planetary and stellar conditions. Our findings show that the large-scale, axisymmetric magnetic field becomes nearly independent of the rotation rate and buoyancy forcing, as characterized by the non-dimensional Ekman number and Rayleigh number, respectively. To the extent that limited parameter space studies may be extrapolated to the more extreme parameter regimes of natural systems, these results suggest that a similar process may be at work in natural dynamos.

As suggested by Malkus & Proctor (1975), our results show that mean and fluctuating magnetic fields saturate through distinct mechanisms. We find that the saturation of the mean magnetic field is the result of the Coriolis-Lorentz force balance that occurs in the zonal component of the mean momentum equation. The corresponding strength of the mean magnetic field is characterized by a mean Elssasser number that is order unity, suggesting that the force balance hypothesis is valid for the large-scale magnetic field. In contrast, the fluctuating magnetic field tends to grow with increasing buoyancy forcing. That the mean magnetic field does not depend on the Rayleigh number in the saturated regime may be understood heuristically by noting that the mean buoyancy force does not enter the zonal component of the mean momentum equation. This finding should be contrasted with the force balance on the fluctuating scales, which is dominated by a leading order geostrophic force balance, and a higher order magnetostrophic balance that involves the buoyancy, Coriolis, Lorentz, and pressure gradient forces (e.g. Yadav et al. 2016). The fact that the fluctuating buoyancy force and the fluctuating Lorentz force are of comparable magnitude may be the reason that the fluctuating magnetic field grows with increasing Rayleigh number.

Applying the present findings to planets and stars requires that the observed magnetic field is separated into mean and fluctuating components. Although Christensen (2010) suggests that the so-called Elsasser number rule (i.e. the Coriolis and Lorentz forces balance and determine the magnetic field strength) does not agree with available numerical data, our findings suggest that this discrepancy is due to the fact that the fields have not been separated into mean and fluctuating components.

Observational studies find that inferred stellar magnetic activity becomes independent of Rossby number below a certain threshold value (Patten & Simon 1996; Mohanty & Basri 2003; Pizzolato et al. 2003; Reiners & Basri 2007). Our findings exhibit some similarity to these studies, though it should be emphasized that the many assumptions that are used in these investigations make it difficult to relate to our numerical findings. In particular, stellar activity is likely tied to small-scale magnetic features arising in the stellar photosphere, a feature not captured in models such as those presented here. It is possible that such small-scale features are directly or indirectly linked to the large-scale, internal magnetic field of the star. The nature of this linkage between large and small scales remains a particularly active area of research, noteably within the context of the Sun (e.g. Hotta, Rempel & Yokoyama 2016).

# **ACKNOWLEDGEMENTS**

This work was supported by the National Science Foundation (NSF) under award numbers EAR-1620649 (MAC), EAR-1945270 (MAC),

and SPG-1743852 (MAC, RJO), and by the National Aeronautics and Space Administration (NASA) under awards 80NSSC17K0008 (NAF) and 80NSSC20K0193 (NAF). The code Rayleigh was developed through the NSF-funded Computational Infrastructure for Geodynamics and supported by NSF award numbers NSF-0949446 and NSF-1550901. This work utilized the RMACC Summit supercomputer, which is supported by the National Science Foundation (awards ACI-1532235 and ACI-1532236), the University of Colorado Boulder, and Colorado State University. The Summit supercomputer is a joint effort of the University of Colorado Boulder and Colorado State University.

## DATA AVAILABILITY

Any data reported within this work is available upon request to the authors.

#### REFERENCES

```
Aubert J., 2005, J. Fluid Mech., 542, 53
Aubert J., Gastine T., Fournier A., 2017, J. Fluid Mech., 813, 558
Aurnou J., King E., 2017, Proc. R. Soc. A, 473, 20160731
Calkins M. A., Orvedahl R. J., Featherstone N. A., 2021, Geophys. J. Int.,
   227, 1228
Christensen U., 2010, Space Sci. Rev., 152, 565
Christensen U., Aubert J., 2006, Geophys. J. Int., 166, 97
Featherstone N. A., Hindman B. W., 2016, ApJ, 818, 32
Hotta H., Rempel M., Yokoyama T., 2016, Science, 351, 1427
Jones C. A., 2011, Annu. Rev. Fluid Mech., 43, 583
Jones C. A., Soward A. M., Mussa A. I., 2000, J. Fluid Mech., 405, 157
Julien K., Knobloch E., Werne J., 1998, Theor. Comput. Fluid Dyn., 11, 251
Kutzner C., Christensen U. R., 2002, Phys. Earth Planet. Inter., 131, 29
Malkus W. V. R., Proctor M. R. E., 1975, J. Fluid Mech., 67, 417
Matsui H. et al., 2016, Geochem., Geophys., Geosystems, 17, 1586
Mohanty S., Basri G., 2003, ApJ, 583, 451
Patten B. M., Simon T., 1996, ApJS, 106, 489
Pizzolato N., Maggio A., Micela G., Sciortino S., Ventura P., 2003, A&A,
   397, 147
Reiners A., Basri G., 2007, ApJ, 656, 1121
Schaeffer N., Jault D., Nataf H.-C., Fournier A., 2017, Geophys. J. Int., 211,
```

Sheyko A., Finlay C., Favre J., Jackson A., 2018, Sci. Rep., 8, 12566
Soderlund K. M., King E. M., Aurnou J. M., 2012, Earth Planet. Sci. Lett., 333, 9
Soderlund K. M., Sheyko A., King E. M., Aurnou J. M., 2015, Prog. Earth Planet. Sci., 2, 24

Stanley S., Glatzmaier G. A., 2010, Space Sci. Rev., 152, 617 Stevenson D. J., 1979, Geophys. Astrophys. Fluid Dyn., 12, 139 Tobias S., 2021, J. Fluid Mech., 912, P1

Wicht J., Christensen U. R., 2010, Geophys. J., 181, 1367

Yadav R. K., Gastine T., Christensen U. R., 2016, Proc. Natl. Acad. Sci., 113, 12065

Yan M., Tobias S., Calkins M., 2021, J. Fluid Mech., 915, A15

This paper has been typeset from a  $\ensuremath{\text{TeX}/\text{IATeX}}$  file prepared by the author.